IAEA FEC 2014: St. Petersburg, Russia, Oct. 13-18, 2014 **Paper: EX/P6-54**

The role of lithium conditioning in achieving high performance, long pulse H-mode discharges in the NSTX and EAST devices

R. Maingi[1], D.K. Mansfield[1], X.Z. Gong[2], Z. Sun[2], M.G. Bell[1], Y.M. Duan[2], H.Y. Guo[3], J.S. Hu[2], R. Kaita[1], S.M. Kaye[1], H.W. Kugel[1], J.G. Li[2], V.A. Soukhanovskii[4], B.N. Wan[2], G.S. Xu[2], and the EAST and NSTX teams

Email: rmaingi@pppl.gov
[1] *Princeton Plasma Physics Laboratory, Receiving 3, Route 1 North, Princeton, NJ 08543 USA*
[2] *Institute of Plasma Physics, Chinese Academy of Sciences, Hefei 230031 China*
[3] *General Atomics, PO Box 85608, San Diego, CA 92186, USA*
[4] *Lawrence Livermore National Laboratory, 7000 East Ave, P.O. Box 808, Livermore CA 94551, USA*

1. Introduction

In this paper, the role of lithium wall conditioning on the achievement of high performance, long pulse discharges in the National Spherical Torus Experiment (NSTX) and the Experimental Advanced Superconducting Tokamak (EAST) is documented. Common observations include recycling reduction and elimination of ELMs. In NSTX, lithium conditioning typically resulted in ELM-free operation[1] with impurity accumulation, which was ameliorated e.g. with pulsed 3D fields to trigger controlled ELMs[2]. Active lithium conditioning in EAST discharges has overcome this problem, producing an ELM-free H-mode with controlled density and impurities[3].

2. NSTX Experiments

Lithium wall conditioning ('dose') was routinely applied onto graphite plasma facing components between discharges in NSTX, partly to reduce recycling[4]. This was accomplished with a pair of toroidally separated overhead lithium evaporators[5]. Initial studies were conducted in discharges with a 'weaker' boundary shaping than typical in NSTX, namely an intermediate-level average triangularity ($\delta \sim 0.46$), low elongation ($\kappa \sim 1.8$), and relatively low squareness shape[6, 7]. Here, we present trends from an experiment in NSTX in which pre-discharge lithium evaporation was systematically increased[8] in highly shaped discharges ($\delta \sim 0.6$-0.7, $\kappa \sim 2.2$, high squareness), as envisioned for NSTX-U.

The global effects of Li evaporation on the highly shaped NSTX discharges are shown in Figure 1, which compares the evolution of a reference ELMy discharge, with an intermediate lithium dose (orange, ELMy), and one with high dose, that stabilized ELMs (blue). The steady P_{NBI} was 6 MW for the reference discharge, compared with 5 MW for the intermediate lithium dose, and 4 MW for the high lithium dose (panel b). Although the reference and intermediate lithium discharges were reasonably well optimized, the highest lithium dose discharge was not fully optimized, due to available run time; this is reflected by the shorter realized pulse length. The rate of increase of line average density dn/dt (panel (c)) from Thomson scattering data was indeed reduced with increasing lithium dose, while the normalized stored energy β_N (panel (d)) was comparable at ~ 6. Here $\beta_N=\beta_t B_t a_m/I_p$, where β_t is the average plasma pressure normalized to the on-axis vacuum toroidal field: $\beta_t=4\mu_0 W_{MHD}/(3V_p B_t^2)$. Also B_t is the toroidal field, a_m the minor radius, I_p the plasma current, W_{MHD} the stored energy from equilibrium reconstructions, V_p the plasma volume, and μ_0 the permittivity of free space. Both the raw energy confinement time τ_E and the value normalized

to the ITERH97L global scaling law increased with lithium dose (H97L shown in panel (e)). As also observed in the weakly shaped discharges, radiated power P_{rad} ramped during long ELM-free periods, which were triggered with the lithium, especially at high doses (panels (f), (g)). Note also the substantial reduction in baseline D_α with lithium. In general, these observations are similar to those made with weaker boundary shaping in NSTX[9-12].

A number of reference ELMy discharges over a range of neutral beam heating were taken prior to the introduction of lithium during this Li dose ramp experiment. The range of pre-discharge dose was from 120 mg to 570 mg; these equate to nominal peak coating thicknesses of ~60-300 nm, i.e. well in excess of the < 10 nm typical ion implantation depth for typical divertor T_e and T_i. Lithium dose in the first seven discharges averaged about 150 mg, and was increased to about 250 mg for the next eight discharges. Finally the dose was increased to about 450 mg for eleven discharges, and then increased to about 550 mg for the last nine discharges of the experiment. In a few instances the dose was lowered between otherwise comparable doses to inspect for signs of hysteresis. Additionally neutral beam power (P_{NBI}) was often modestly reduced with increasing dose, because the increase in confinement would otherwise have resulted in exceeding of the global beta limit, and subsequent minor or major disruption. Note that the reference non-lithiated discharges used standard inter-discharge Helium Glow Discharge Cleaning for reproducibility, which was not needed after lithium was introduced.

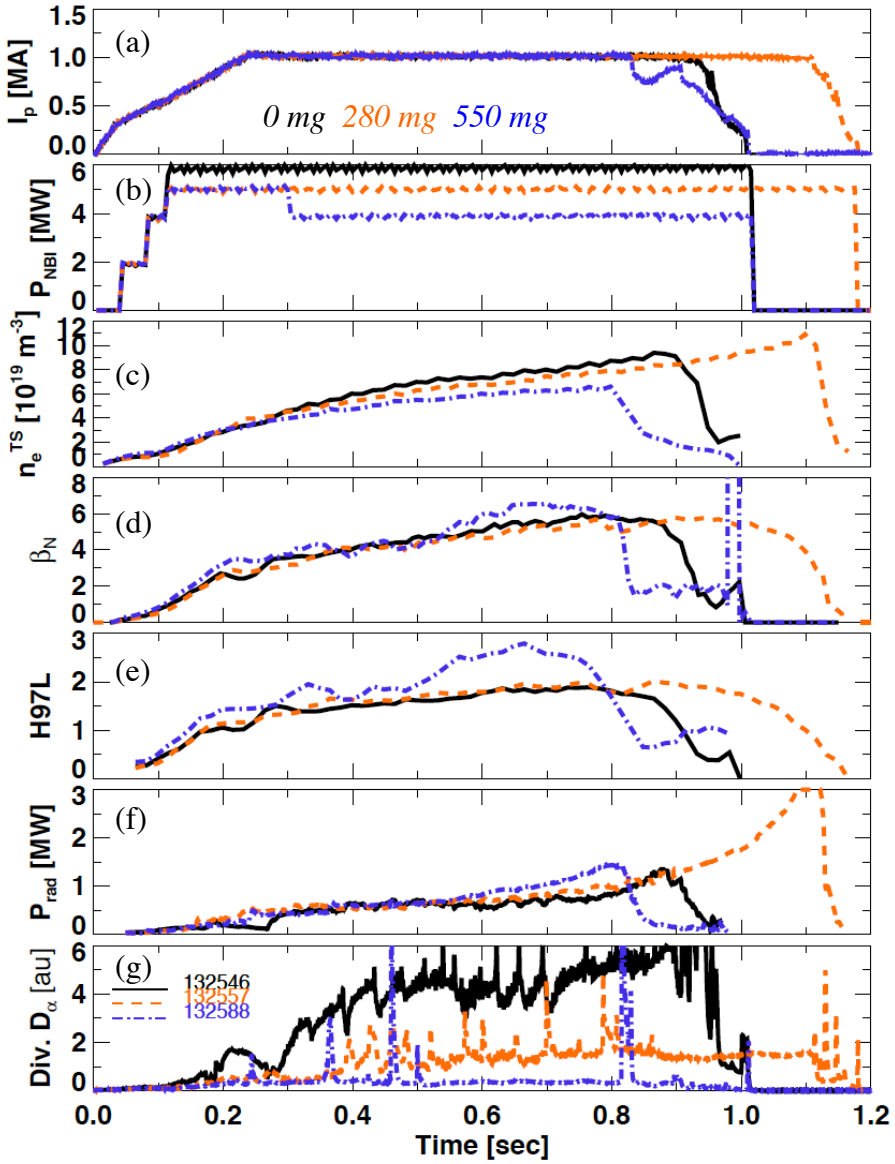

Figure 1: Impact of low (280 mg) and high (550 mg) pre-discharge Li dose with reference non-lithiated discharge in NSTX.

Figure 2 shows the trends of lower and upper divertor D_α, confinement relative to H97L

scaling, and midplane neutral pressure with increasing lithium dose. The plots are color coded: the orange stars are from the present high shaping study, while the black diamonds are from the previous study in weakly shaped discharges[12]. The trends are, overall, rather comparable. A few points are noted. First, both datasets show a sharp decrease in lower divertor D_α, followed by a flattening at higher lithium dose (panel (a)). We interpret this as the transition from the high recycling to sheath-limited heat transport regimes. This transition occurs at lower lithium dose for the highly shaped discharges than the weakly shaped ones.

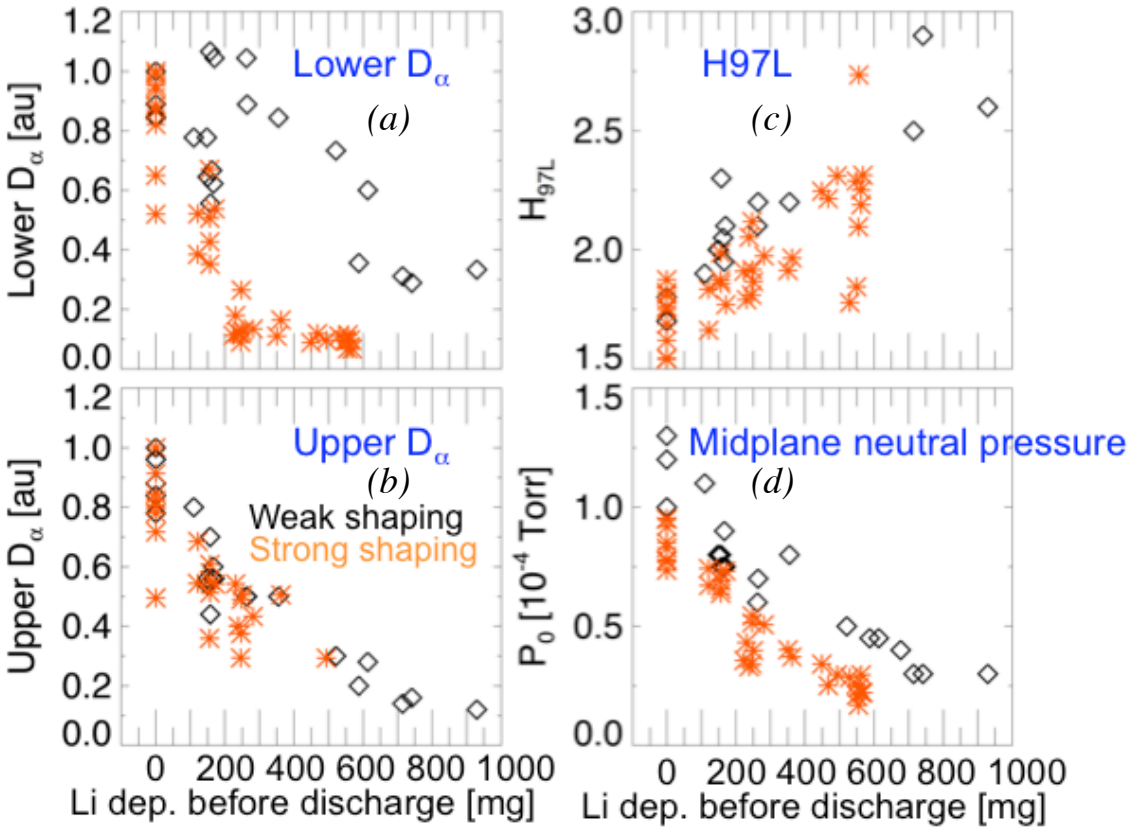

Figure 2: Dependence of various quantities on pre-discharge lithium evaporation: (a) lower divertor D_α, (b) upper divertor D_α, (c) confinement relaive to H97L scaling, and (d) midplane neutral pressure. High and low δ discharges are color-coded. Panels (a), (b), and (c) are taken near 300msec, while panel (c) is evaluated at the peak of the stored energy during each discharge.

This is qualitatively consistent with expectations, in that the strongly shaped discharges have the centroid of lithium deposition much closer to the outer strike point than the weakly shaped discharges. The final fractional reduction in lower divertor D_α is also larger in the highly shaped discharges (90% reduction, compared with ~ 70% in the weakly shaped discharges). There are other factors related to the X-point geometry, but these differences seem qualitatively understandable. Second, the relative confinement improvement trend is similar, but the magnitude may be slightly lower in the highly shaped discharges than in the lower shaped discharges (panel (c)). Additional data, including data at higher lithium doses, would be needed to determine if there were a real difference in the trends; for now, the plan is to conduct experiments over a wide range of lithium dose in NSTX-U. Finally the magnitude of the neutral pressure is markedly lower (by up to 50%) in the highly shaped discharges. The highly shaped discharges were closer to true double-null configuration, and thus may have

had better isolation between the midplane and divertor than the lower shaped discharges, which were biased more strongly toward the lower divertor.

In addition to the global changes, the upstream plasma profiles change with increasing lithium dose in the highly shaped discharges. These changes are illustrated for three discharges with differing lithium dose (Figure 3), as a function of normalized poloidal flux ψ_N, where $\psi_N = (\psi_0 - \psi(r))/(\psi_0 - \psi_{sep})$ with ψ_0 and- ψ_{sep} being the poloidal flux at the magnetic axis and separatrix respectively. The yellow arrows in the figure represent increasing lithium dose. Panel (a) shows that the n_e profile shifts inward with increasing lithium dose, while panel (b) shows that the T_i increases with increasing dose. Panel (c) shows that the near-separatrix T_e drops a little with increasing lithium dose, but that the T_e value for $\psi_N < 0.9$ increases substantially. The kinetic profiles were fit with 'standard' modified hyperbolic tangent functions, using a set of algorithms that allow selection of profiles as a function of the ELM cycle. These fitted profiles for the total pressure are shown in panel (d): it can be seen that the far edge pressure decreases with increasing dose, whereas the pressure for $\psi_N < 0.85$ increases substantially. This is similar to studies from the lower shaped discharges, which indicated improved edge stability with similar profile changes[7, 11]. In the previous studies, the individual density and temperature profiles changes appeared to be correlated to micro-tearing and electron temperature gradient mode stability[13]; it is likely that similar physics is present in the highly shaped discharges.

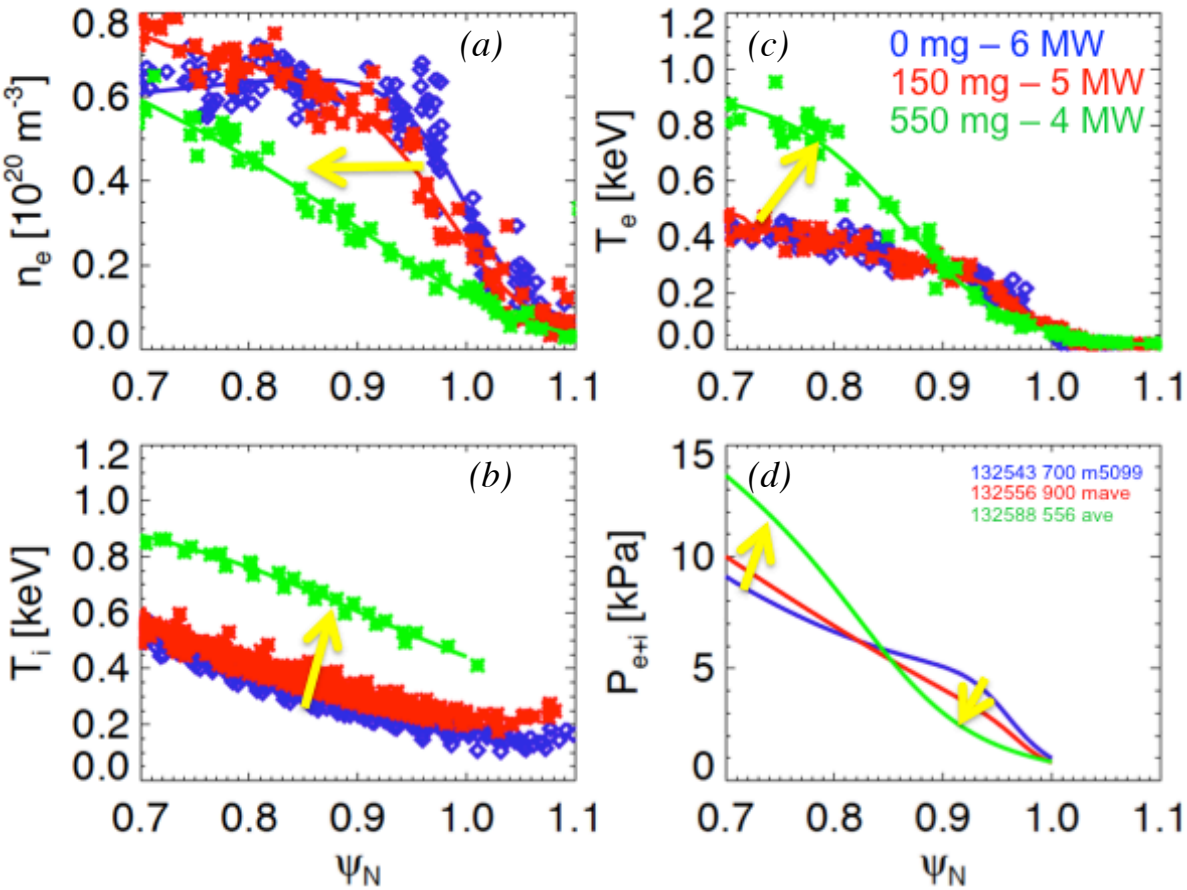

Fig. 3: Edge profiles for three discharges with different levels of Li dose, with increasing dose indicated by yellow arrows. Note also the modest differences in NBI heating power.

The ultimate advantage of the highly shaped discharges is improved global stability limits. Hence these discharges could withstand 4-5 MW of heating power, leading to high pedestal pressures. In comparison, the less shaped discharges were limited to 2-3 MW of NBI power and lower pedestal pressures[8]. These experiments bode well for the coming Li evaporation experiments planned for NSTX-U operation, which will commence in 2015.

3. EAST Experiments

In EAST[14] extensive lithium wall conditioning is done via evaporators[15] prior to a run day, and this was integral to achievement of the first[16] and record long H-modes[17] and L-modes[18]. During the course of a run day, the state of the lithium coating can vary, and thus active conditioning during plasma discharges via a lithium aerosol injector[19] was sometimes employed for real time conditioning.

The lithium injector uses a resonating piezoelectric disk with a central aperture to release microscopic spherical droplets diameter (~ 45 μm) into the plasma scrape-off layer. Li injection rates from ~1-120 mg/s (4.3×10^4 - 5.1×10^6 spheres/sec) can be attained reproducibly using this device. In these experiments, Li aerosol was injected through the upper divertor gap into the upper X-point of H-mode discharges at ~ 47 mg/sec (~ 2×10^6 spheres/s, ~ 4×10^{21} atoms/s). The velocity of the aerosol is gravitationally driven, reaching ~ 9 m/sec when the particles reach the SOL plasma.

Figure 4 compares the evolution of a discharge with active lithium aerosol injection for 18 seconds (as indicated by the vertical arrows of the red discharge), with a subsequent reference

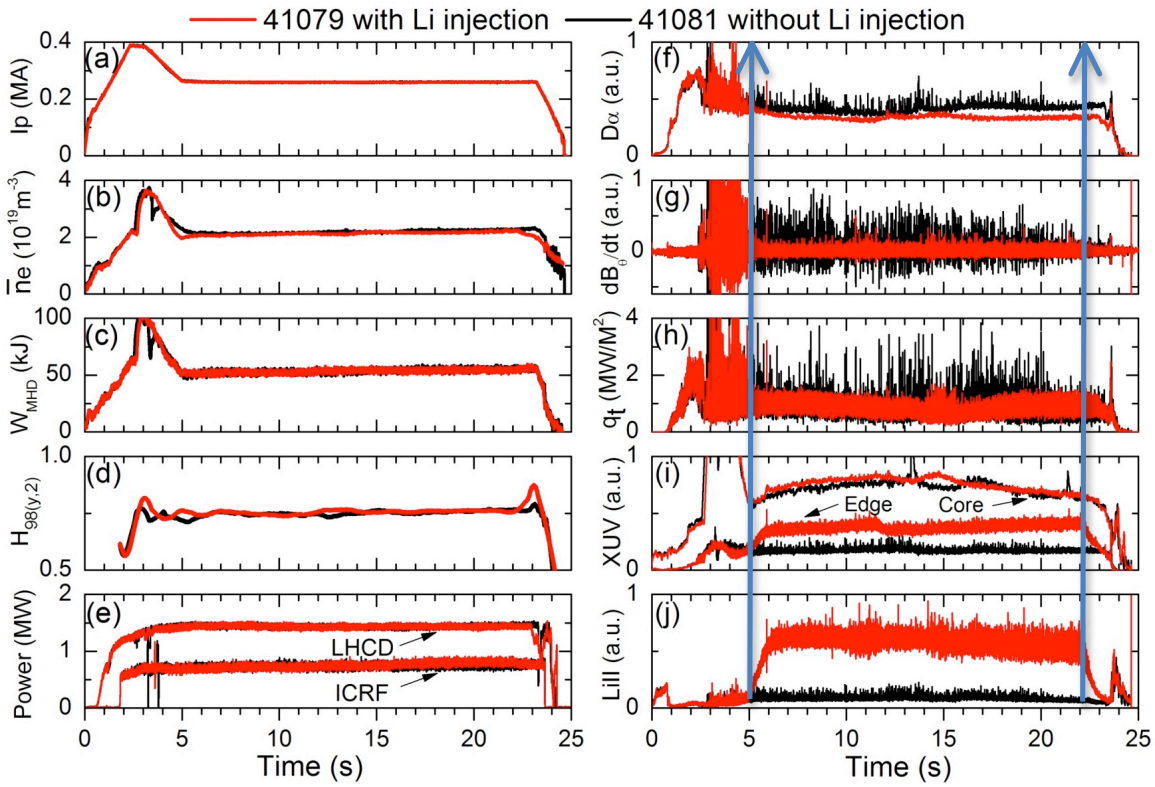

Figure 4: Evolution of discharge parameters for a reference ELMy discharge (black) and one with active lithium conditioning (red) in EAST: (a) plasma current, (b) line average density, (c) stored energy, (d) energy confinement relative to H98y2 scaling, (e) heating power from LH and ICRF, (f) divertor D_α emission, (g) magnetic probe signal, (h) divertor heat flux from Langmuir probes, (i) edge and core XuV emission, and (j) Li-III emission.

no-Li discharge[20]. As can be seen, there was little change in density, stored energy and confinement, at constant input power. The recycling increased modestly in the reference Li discharge, with the resumption of ELMs apparent in panel (f). The magnetic fluctuations associated with the ELMs were eliminated, but the fluctuation level between ELMs was unaffected (panel (g)). The inter-ELM target heat flux was mostly unaffected, although the ELM related heat flux peaks were eliminated (panel (h)). The edge extreme ultraviolet (XUV) emission was increased due to the presence of Li in the edge, but the core was little affected (panel (i)). Finally very little Li was present in the discharge without Li injection (panel (j)). As in NSTX, large ELMs were eliminated. The radiated power and soft X-ray emission at the edge was indeed higher in the discharge with real-time Li injection. However, the plasma density was well controlled, without impurity accumulation in the core plasma, in contrast to the NSTX observations.

Real-time Li injection was carried out for five consecutive discharges, with one of those discharges having an unplanned reduction in LH power. Figure 5 compares the evolution of D_α from the lower divertor (inboard and outboard) and the upper divertor (inboard and outboard) by averaging multiple spectroscopic sightlines that look through those regions. Recycling, as indicated by D_α emission, dropped promptly in all sightlines with commencement of Li injection, and large ELM activity ceased. The magnitude of the reduction varied from 20-40%, and a couple of discharges were required to reach the lowest baseline D_α emission levels. We note that there appears to be some hysteresis in terms of the effect of Li injection on recycling. As compared to the prompt drop in D_α when Li wsa initiated (shown in Figure 5), the increase of D_α when Li was ceased seems to have occurred

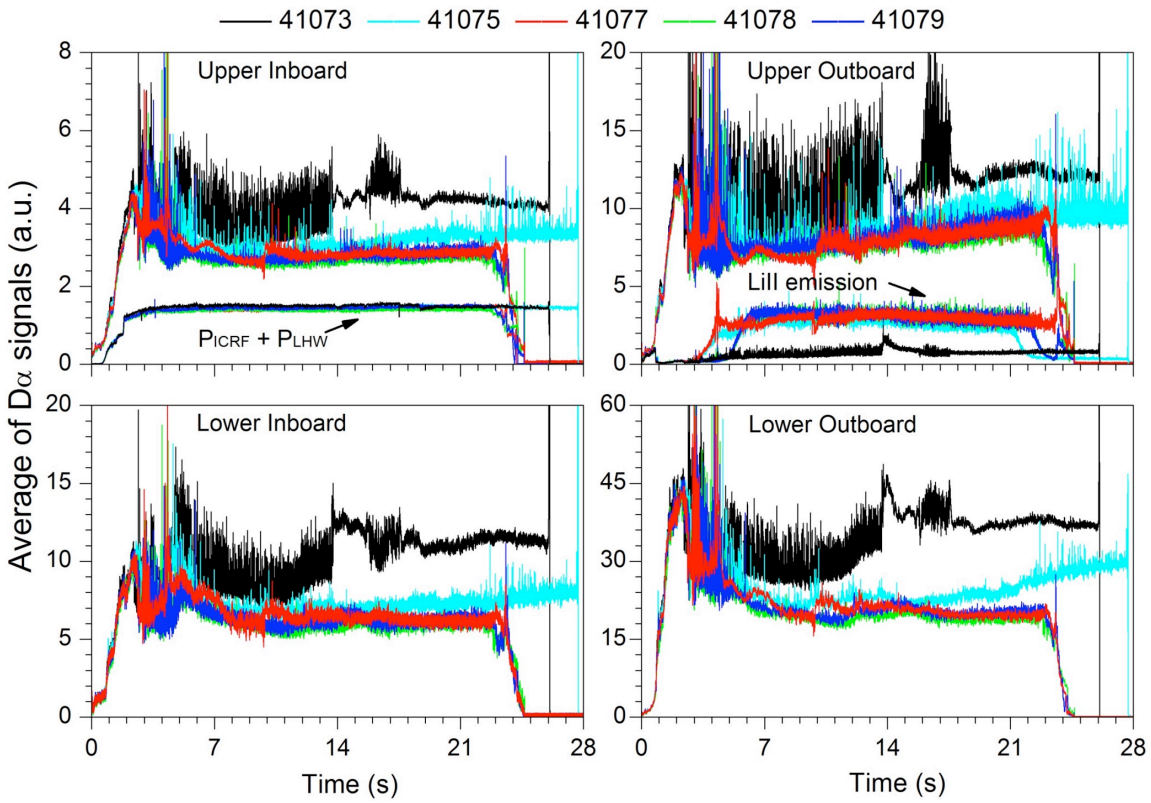

Figure 5: Evolution of D_α emission during five discharges in EAST. The first was a reference no-Li discharge, whereas the subsequent discharges utilized active Li injection. Recycling light is observed to drop in all divertor regions.

more slowly, e.g. panel 4f shows the D_α increased by about 10% two discharges after Li injection was ceased.

The cessation of ELM activity was strongly correlated with the timing of the Li injection, as shown in Fig. 6 from the first discharge with active Li injection. The time for complete ELM elimination was a few sec. Similarly the resumption of ELMs correlated temporally with the termination of Li injection, indicating a causal relationship (Figure 6).

Recent analysis[3] has shown that the Li injection promotes the growth of a medium frequency (~45 kHz) edge coherent mode[21], which is thought to be responsible for providing additional transport that results in ELM elimination. This may be attributed to increased edge collisionality due to the presence of Li in the edge plasma.

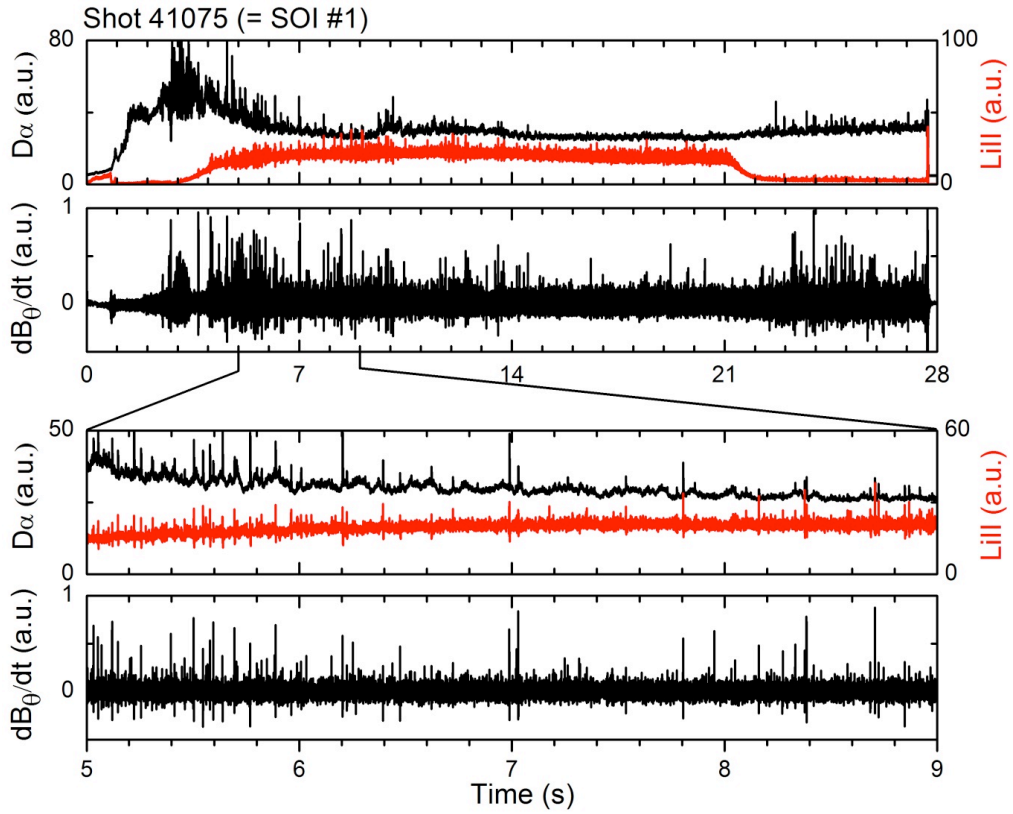

Figure 6: expanded time base for first discharge with Li injection showing cessation(resumption) of ELMs with initiation (termination) of Li injection in EAST. Large ELMs were eliminated gradually over several sec.

4. Discussion, Summary, and Future Work

In summary, the results from both devices demonstrate the common benefits of lithium conditioning. In both devices, Li conditioning reduced baseline D_α emission and completely eliminated ELMs, despite the differing delivery methods (NSTX with evaporators, EAST with active Li injection in the discharges presented here). There is a striking difference worth noting: while the use of Li in NSTX reduced edge transport and turbulence[10], it clearly enhanced edge transport via enhanced coherent mode activity in EAST. This latter observation bears some resemblance to the recent active Li injection in DIII-D with a similar Li dropper device, which also stimulates a coherent mode that changes the edge profiles and

enhances edge stability[22].

Ultimately, the new observation of a quasi-steady discharge devoid of large ELMs with constant radiated power in EAST improves the prospects for the applicability of lithium conditioning for future long-pulse devices, removing one of the obstacles to progress toward steady state discharges in NSTX experiments. Collaborative experiments for systematic comparisons will continue in EAST and the new NSTX-U device to further explore this exciting regime enabled by active Li injection.

Acknowledgements

*Research sponsored in part by the U.S. Dept. of Energy under contract DE-AC02-09CH11466 and in part by the National Nature Science Foundation of China under Contract No. 11021565 and the National Magnetic Confinement Fusion Science Program of China under Contract Nos. 2010GB104001, 2010GB104002, 2011GB101000, 2011GB107001, 2012GB101001, 2013GB107003 and 2013GB106003, the JSPS-NRF-NSFC A3 Foresight Program in the field of Plasma Physics (NSFC No 11261140328), as well as the Thousand Talent Plan of China.

References

1 Bell M. G. *et al*., Plasma Phys. Control. Fusion **51**, 124054 (2009).
2 Canik J. M. *et al*., Phys. Rev. Lett. **104**, 045001 (2010).
3 Hu J. S., Phys. Rev. Lett., submitted (2014).
4 Kugel H. W. *et al*., Phys. Plasmas **15**, 056118 (2008).
5 Kugel H. W. *et al*., J. Nucl. Mater. **390-391**, 1000 (2009).
6 Mansfield D. K. *et al*., J. Nucl. Mater. **390-391**, 764 (2009).
7 Maingi R. *et al*., Phys. Rev. Lett. **103**, 075001 (2009).
8 Maingi R. *et al*., J. Nucl. Mater., submitted (2014).
9 Maingi R. *et al*., Phys. Rev. Lett. **107**, 145004 (2011).
10 Canik J. M. *et al*., Phys. Plasmas **18**, 056118 (2011).
11 Boyle D. P. *et al*., Plasma Phys. Control. Fusion **53**, 105011 (2011).
12 Maingi R. *et al*., Nucl. Fusion **52**, 083001 (2012).
13 Canik J. M. *et al*., Nucl. Fusion **53**, 113016 (2013).
14 Wan B. N., J.G. Li, and Guo H. Y., Nucl. Fusion **53**, 104006 (2013).
15 Zuo G. Z. and Hu J. S., J. Nucl. Mater. **438**, S90 (2013).
16 Xu G. S. *et al*., Nucl. Fusion **51**, 072001 (2011).
17 Li J. *et al*., Nature Phys. **9**, 817 (2013).
18 Guo H. Y. *et al*., Nucl. Fusion **54**, 013002 (2014).
19 Mansfield D. K. *et al*., Fusion Eng. Des. **85**, 890 (2010).
20 Hu J. S., J. Nucl. Mater., submitted (2014).
21 Wang H. Q. *et al*., Phys. Rev. Lett. **112**(2014).
22 Jackson G. L., Proc. 25th IAEA Fusion Energy Conf., St. Petersburg, Russia, Oct. 13-18, 2014, submitted (2014).